

THEORETICAL STUDIES OF DeNO_x SCR OVER Cu-,
Fe- AND Mn-FAU CATALYSTSIzabela Kurzydym¹, Izabela Czekaj¹, ✉<https://doi.org/10.23939/chcht15.01.016>

Abstract. *Ab initio* calculations based on the density functional theory were used. A cluster model of the faujasite zeolite structure (Al₂Si₂₂O₆₆H₃₆) with metal particles adsorbed above the aluminium centres was used. The NO and NH₃ adsorption processes, individual and co-adsorption, have been studied over metal nanoparticles bound into zeolite clusters. Several configurations, electronic structure (charges, bond orders) and vibration frequencies have been analyzed to determine feasible pathways for the deNO_x reaction. The M₂O dimers (M = Cu, Mn or Fe) were considered in relation to the previous studies of iron complexes.

Keywords: zeolites, FAU, deNO_x, vibrational structure, SCR, cluster model.

1. Introduction

Environmental protection plays an important role in sustainable development. One of the problems associated directly with environmental protection is the presence of harmful pollutants in air [1]. Nitrogen oxides (NO_x) have a negative influence on human life and health, and due to the solar radiation they form the so-called photochemical smog. Nitrogen oxides may be present in effluent gases from various sources: automotive, energy, and heavy industry. In the literature reports, the Cu modified zeolites have revealed a high activity in the deNO_x reaction [2]. In this study we present theoretical results on the mechanism of deNO_xSCR over Cu-, Fe- and Mn-FAU catalyst.

All three metal centres within the zeolite framework have been studied extensively both experimentally and computationally. The most widely used zeolite catalysts are the iron based Fe-ZSM-5 [3-6] and copper-exchanged zeolites with the chabazite structure [7, 8].

The iron-exchanged zeolite (mainly ZSM-5) is an active catalyst for a large number of reactions, of which

the selective catalytic reduction (SCR) of nitrogen oxides with ammonia or hydrocarbons [9-13], the N₂O decomposition reaction [14, 15] and oxidation processes [16-19] are the most important.

The structure and exact role of the active iron sites in these different catalytic reactions are still subjects of many discussions. For the SCR of NO_x, different active iron sites, such as small oxygen-bridged clusters [Fe-O-Fe] or [HO-Fe-O-Fe-OH]²⁺ [20-23], isolated Fe²⁺ and Fe³⁺ ions [24], or extraframework Fe-O-Al and grafted Fe-O-Si species [25, 26] have been suggested. The previous studies suggest that all of these iron species usually coexist in the pores of the zeolite framework; however, binuclear iron and isolated iron species have been suggested to be the most active sites for the SCR [37-31].

The copper zeolites are particularly attractive due to their hydrothermal stability. Different studies agree that the major active species are single Cu(II) or Fe(III) centres located in the 6-membered or 8-membered rings of the zeolite framework, where they balance the negative charge of the Al³⁺ site. Depending on the coordination of further ligands such as water, NH₃, or NO, as well as on temperature, the Cu centres can detach from the zeolite framework and become mobile [32-37]. On the other hand, the Fe centres are believed to be more strongly bound and remain immobile within the zeolite framework [38].

In the case of manganese the studies on a support different from zeolite have been extensively reported, both experimental and theoretical ones; they found out a high potential of manganese for the SCR reaction.

The literature data show that manganese oxides supported on TiO₂ [39-41] and Al-SBA-15 [42] as well as Mn-containing activated carbons [43] are active catalysts in the SCR of NO. However, they are deactivated at a high temperature. The Cu-promoted zeolites were found to be less prone to deactivation and highly selective to N₂. However, they were not effective enough during the initial phase of operation when a car engine and a catalyst are cold [44, 45]. Baran *et al.* [40] studied the properties of MnSiBEA and MnAlBEA catalysts obtained from the parent BEA zeolite by a two-step post-synthesis method developed by Dzwigaj *et al.* [46, 47] and by the conventional wet ion-exchange, respectively. In the

¹ Faculty of Chemical Engineering and Technology,
Cracow University of Technology,
24, Warszawska St., Kraków, 31-155, Poland
✉ izabela.czekaj@pk.edu.pl
© Kurzydym I., Czekaj I., 2021

zeolites obtained by the two-step post-synthesis method with a low metal content, manganese is present in the framework positions as Mn(II) and Mn(III). They show that the location of the manganese species, their oxidation state as well as acidity played an important role in NH₃-SCR.

Xu *et al.* [48] studied two series of Mn/beta and Mn/ZSM-5 catalysts, which were prepared to study the influence of different Mn precursors on the selective catalytic reduction (SCR) of NO by NH₃ at low reaction temperatures. The excellent catalytic performance was ascribed to the enrichment of highly dispersed MnOx (Mn₂O₃ and MnO₂) species that act as an active phase in the NH₃-SCR process.

Even though many details of the catalytic mechanism have been elucidated, the SCR mechanism is still not fully understood [49, 50]. This is particularly true for the Fe-exchanged zeolite catalysts which have been studied less extensively than the Cu-exchanged zeolite catalysts. Although for the Cu catalysts computational studies explored different possible mechanistic pathways [50-53], a comprehensive computational picture of the SCR mechanism for Fe and Mn catalysts is still lacking [54, 55], especially in the case of manganese-zeolite supported catalysts.

Here, we aim to fill this gap by computationally exploring different NO and NH₃ adsorption scenarios necessary for the SCR reaction with Cu, Fe and Mn within the FAU zeolite catalysts, which provides a unified picture of NO and NH₃ adsorption and coadsorption in the case of different transition metals.

2. Experimental

2.1. Computational Details

The electronic structure of all clusters was calculated by *ab initio* density functional theory (DFT) methods (StoBe program, [56]) using the non-local generalized gradient corrected functionals according to Perdew, Burke, and Ernzerhof (RPBE) [57, 58], in order to account for the electron exchange and correlation. All Kohn-Sham orbitals are represented by linear combinations of atomic orbitals (LCAO's) using contracted Gaussian basis sets for the atoms [59, 60]. A detailed analysis of the electronic structure of the clusters was carried out using Mulliken populations [61] and Mayer bond order indices [62, 63].

A double zeta valence polarization (DZVP) type was used for the orbital basis sets of Sn (633321/53321/531), Fe, Mn and Cu (63321/531/311), Si (6321/521/1), Al (6321/521/1), O, C (621/41/1), and H (41). Auxiliary basis sets, such as (5,5;5,5) for Si, Sn and Fe, (4,3;4,3) for O, C, N, and (41) for H, were applied to

fit the electron density and the exchange-correlation potential.

The vibration frequencies of the adsorbed molecules were calculated by single point energy calculations of the optimized geometries. The calculations of the vibrational frequencies were performed with harmonic approximations as well as an anharmonicity fit in the Morse potential function, as implemented into the StoBe code [64]. The frequencies are reported as obtained from the calculations, without scaling.

The adsorption energy of individual structures was calculated according to the formulae below.

The adsorption energies of the adsorbates on the cluster were calculated as follows:

$$E_a(\text{adsorbate/cluster}) = E_{\text{tot}}(\text{adsorbate/cluster}) - E_{\text{tot}}(\text{cluster}) - E_{\text{tot}}(\text{adsorbate}) \quad (1)$$

where $E_{\text{tot}}(\text{adsorbate/cluster})$ is the total energy of the adsorbate/cluster surface complex, $E_{\text{tot}}(\text{cluster})$ and $E_{\text{tot}}(\text{adsorbate})$ are the total energies of pure cluster and the adsorbate, respectively.

The calculations took into account the structures with the lowest energy (for each structure all probable multiplicity were calculated):

1. Adsorption energy of metallic dimer on the structure of faujasite zeolite:

$$E_a = E_{\text{FAU_MOM}} - E_{\text{FAU}} - E_{\text{MOM}} \text{ [eV]} \quad (2)$$

2. Nitric oxide adsorption energy on metallic dimer deposited on the structure of faujasite zeolite:

$$E_a = E_{\text{FAU_MOM_NO}} - E_{\text{FAU_MOM}} - E_{\text{NO}} \text{ [eV]} \quad (3)$$

3. Ammonia adsorption energy on metallic dimer deposited on the structure of faujasite zeolite:

$$E_a = E_{\text{FAU_MOM_NH}_3} - E_{\text{FAU_MOM}} - E_{\text{NH}_3} \text{ [eV]} \quad (4)$$

4. Co-adsorption energy of nitric oxide and ammonia on metallic dimer deposited on the structure of faujasite zeolite:

$$E_a = E_{\text{FAU_MOM_NO_NH}_3} - E_{\text{FAU_MOM}} - E_{\text{NO}} - E_{\text{NH}_3} \text{ [eV]} \quad (5)$$

2.2. Geometrical Model

The crystal structure of FAU and MFI has been chosen from the Database of Zeolite Structure [65]. The cubic phase of FAU (Fig. 1) framework type is described by the space group Fd-3m (# 227) with lattice constants $a=b=c=24.3450 \text{ \AA}$. The crystal unit cell contains 706 atoms. The faujasite framework consists of sodalite cages that are connected with hexagonal prisms. A pore, which is formed by a 12-membered ring, has a relatively large diameter of 7.4 \AA . The inner cavity has a diameter of 12 \AA and is surrounded by 10 sodalite cages.

A cluster model of faujasite (Al₂Si₂₂O₆₆H₃₆) zeolite structure was used with M particles (M=Cu, Mn or Fe) adsorbed above the aluminium centres in the faujasite frame (Fig. 1). The oxidized M₂O dimers were considered in relation to the previous studies of iron complexes [18].

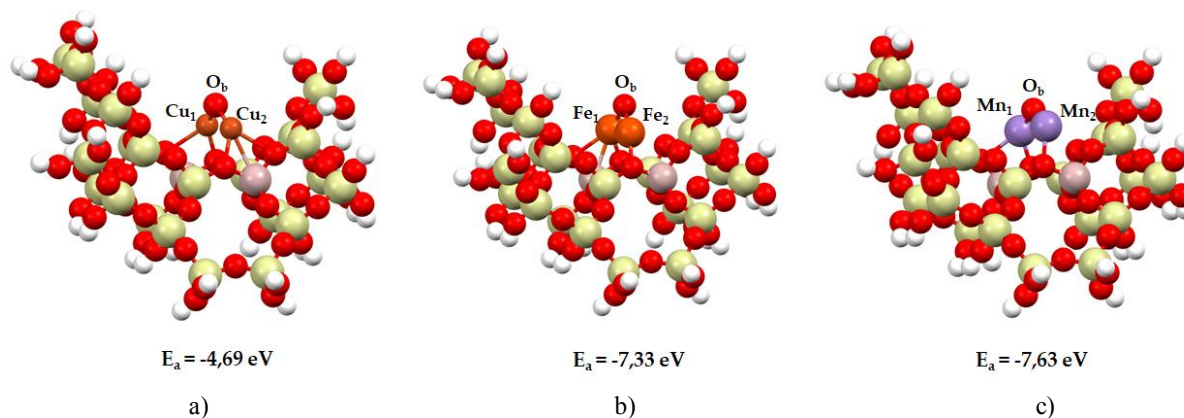


Fig. 1. Cluster model of faujasite ($\text{Al}_2\text{Si}_{22}\text{O}_{66}\text{H}_{36}$) zeolite structure with deposited metallic dimmers: copper dimer (a), iron dimer (b) and manganese dimer (c) with the adsorption energy below structure

3. Results and Discussion

During the studies a fragment of the faujasite zeolite with the $\text{Al}_2\text{Si}_{22}\text{O}_{66}\text{H}_{36}$ structure was selected for calculations, which well reflects the active centres in the catalyst. Subsequently, structures with embedded copper, iron and manganese dimers were designed (Fig. 1); the dimer, apart from two metal atoms, also contained a bridged oxygen atom connecting the metal atoms. The stabilization of M-Ob-M dimer complexes (where M = Cu, Fe and Mn) on the designed structure was tested. All the analyzed systems showed stabilization near aluminium atoms within the zeolite framework *via* metal-oxygen bond. The oxygen atom to which the dimer attached is adjacent to the aluminium atoms in the structure. In addition, the adsorption energy calculated for all deposited dimers showed that the attachment is exothermic. Iron and manganese interact more strongly with the zeolite structure by releasing more energy during adsorption: -7.33 eV for the iron dimer and -7.63 eV for the manganese dimer. Much less energy is released while adsorbing the copper dimer: -4.69 eV. In the analysis of the length and bond orders in the embedded dimers a significant interaction of Fe-Fe (bond order 1.215) should be noted, compared with almost negligible interactions of Cu-Cu and Mn-Mn (0.232 and 0.107, respectively). The M-Ob bond lengths for each metal are comparable and range within 1.81–1.86 Å.

The next stage was the adsorption of nitric oxide and ammonia and the co-adsorption of nitric oxide with ammonia on stable zeolite structures with embedded metal dimers (Figs. 2-4). These reactions form the basis for further research on the mechanism of the SCR process for a selected catalyst. Calculation of adsorption energy based on the optimized structures allowed to state that in all cases we are dealing with exothermic adsorption, which suggests that these processes should occur spontaneously without energy barrier (without the necessity of supplying additional energy to the system). In all cases it can also be

noticed that the co-adsorption of nitric oxide and ammonia is more exothermic than the adsorption of single molecules – nitric oxide or ammonia. The most energy is released during co-adsorption on the structure with an iron dimer: -2.97 eV, next on the structure with a manganese dimer: -2.56 eV, and the least energy is obtained in the case of adsorption on the structure with a copper dimer: -1.99 eV. Comparing the energies of the adsorption of nitric oxide and ammonia we may notice that the adsorption of nitric oxide proceeds with the release of more energy than in the case of the adsorption of ammonia, which indicates a stronger bond of the nitric oxide with the catalyst structure. The strength of this adsorption can have a significant impact on further SCR processes and, consequently, on the formation of N_2 and H_2O molecules. The mechanism of attachment of nitric oxide, which differs depending on the type of metal in the dimer is also worth noticing here. In all cases, ammonia attaches to one of the metal atoms in the dimer. The same principle of attachment is also observed in the co-adsorption. Nitric oxide in the copper dimer binds through the bond formed between nitrogen and bridge oxygen. In other two dimers – iron and manganese – nitric oxide combines with the dimer by forming a bond between nitrogen and a metal atom.

In the further stage of the work, an analysis of charges for dimers and the molecules adsorbed on them was carried out (Fig. 5). This analysis explains the difference in the attachment of nitric oxide to the copper dimer. The nitrogen atom when attached to the copper dimer increases its charge, which is positive in the free nitric oxide molecule (and changes from 0.045 to 0.243). In the case of the iron and manganese dimer, the charge on the nitrogen atom in nitric oxide is converted from positive to negative, thus the attachment to the negative bridge oxygen atom is not possible and nitrogen oxide attaches to the metal atom. In addition, the negativity of charge on the nitrogen is slightly higher for the manganese dimer (-0.067) compared to the iron dimer (-0.017).

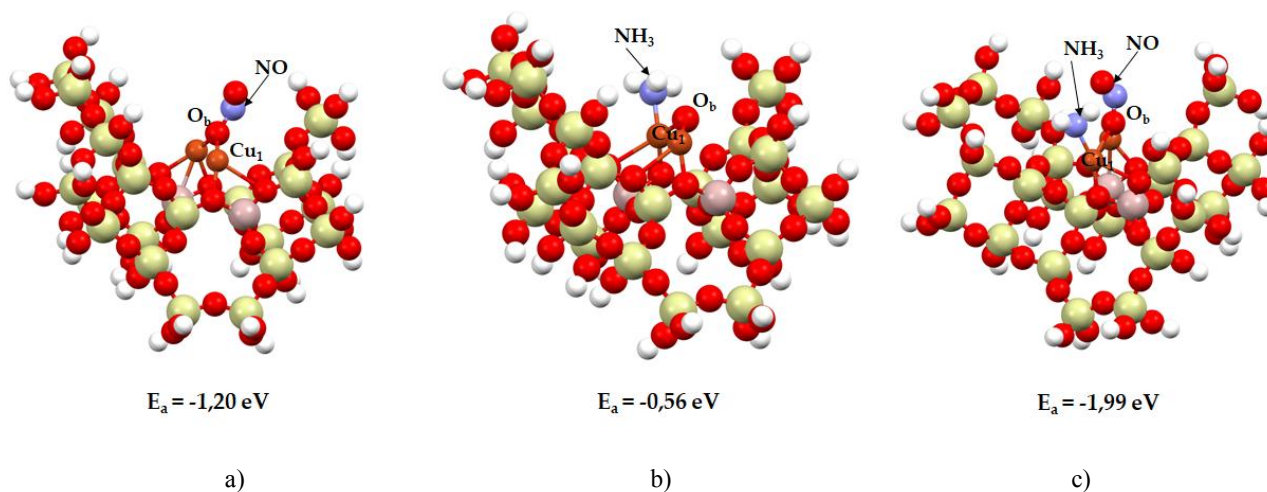


Fig. 2. Visualization of adsorption of nitric oxide (a), ammonia (b) and co-adsorption of nitric oxide and ammonia (c) on faujasite with copper dimer with adsorption energy below structure

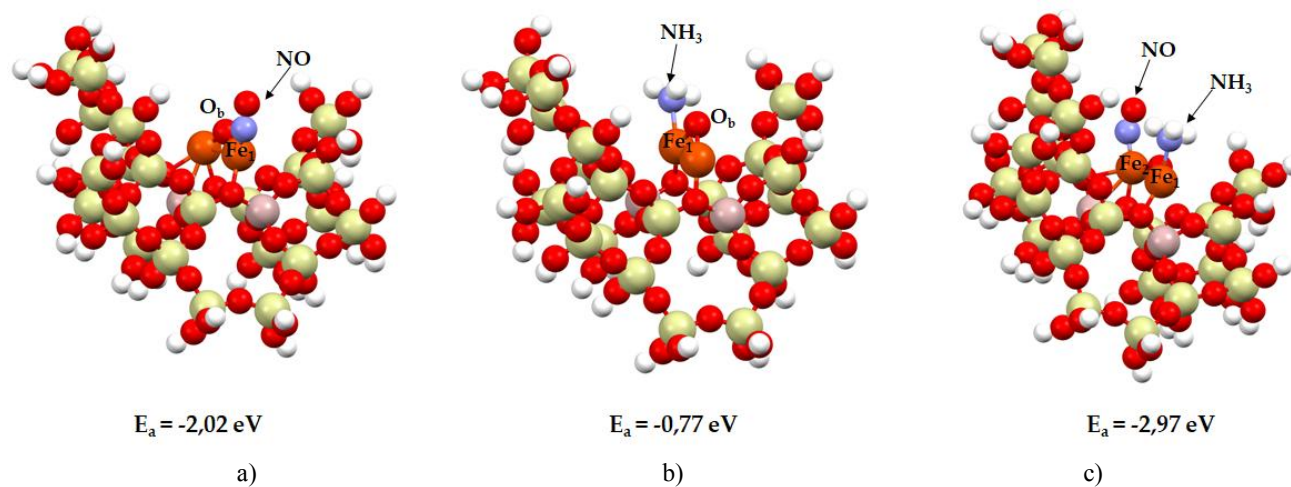


Fig. 3. Visualization of adsorption of nitric oxide (a), ammonia (b) and co-adsorption of nitric oxide and ammonia (c) on faujasite with iron dimer with adsorption energy below structure

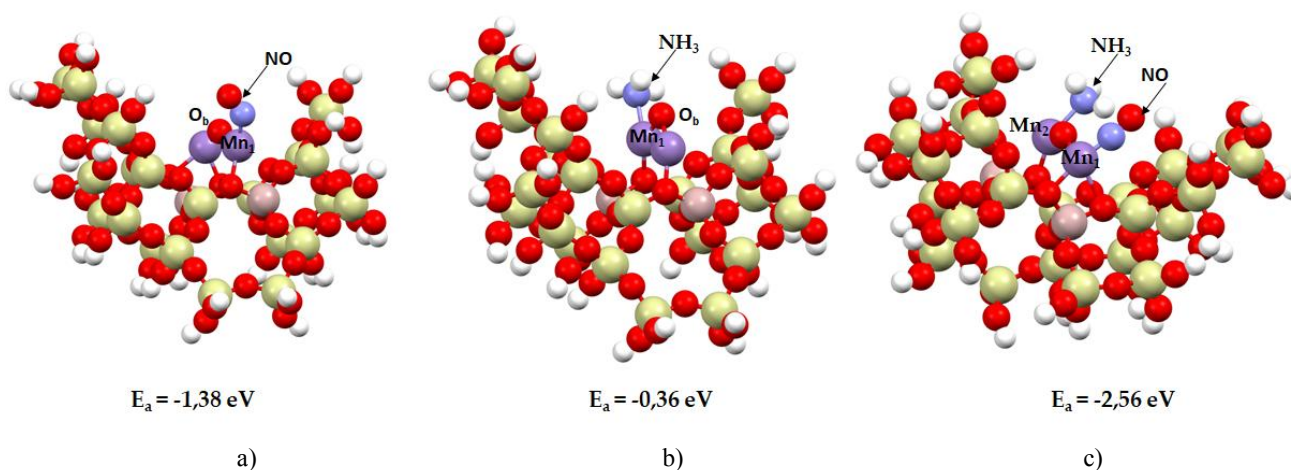


Fig. 4. Visualization of adsorption of nitric oxide (a), ammonia (b) and co-adsorption of nitric oxide and ammonia (c) on faujasite with manganese dimer with adsorption energy below structure

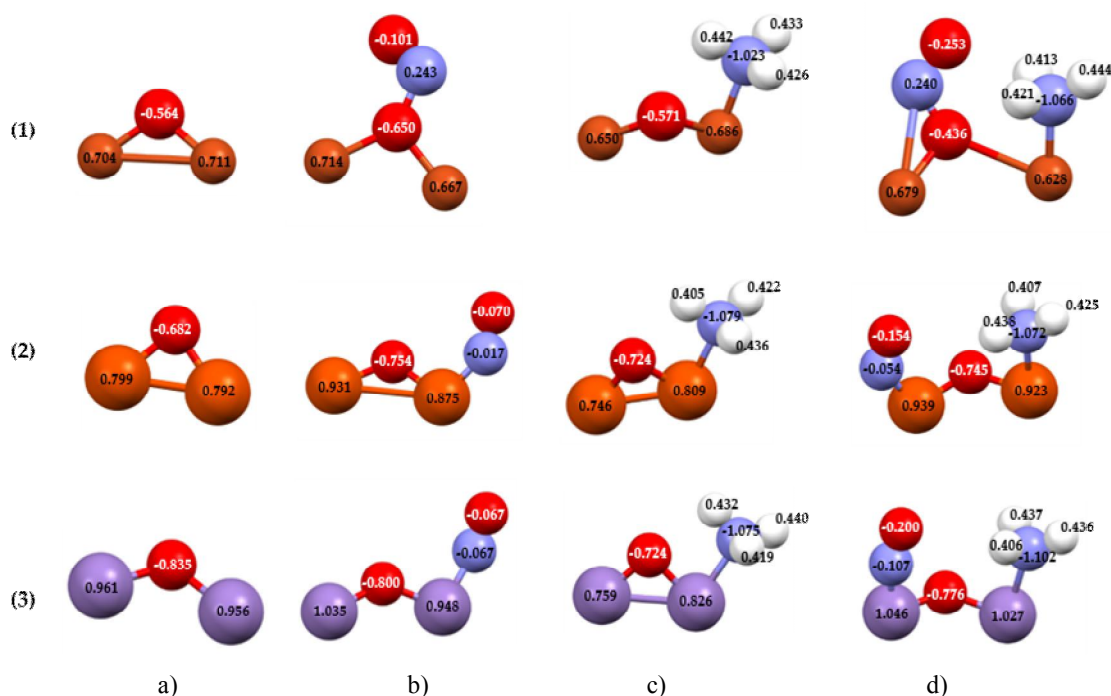


Fig. 5. Charge distribution for metallic dimers: copper (1), iron (2) and manganese (3). Metal dimers (a), nitric oxide adsorption (b), ammonia adsorption (c), nitric oxide and ammonia adsorption (d)

Analyzing the charges on the hydrogen and nitrogen atoms in ammonia it can be noticed that the redistribution of charge occurred compared to the free ammonia molecule. In the free ammonia molecule the charge on the nitrogen atom amounts to -0.940, whereas on the hydrogen atoms 0.314. After the adsorption of ammonia on the metallic dimer, the hydrogen atoms have a more positive charge (on the average 0.43), while the nitrogen atom has a more negative charge (on the average -1.08). The same tendency can be noticed in the case of co-adsorption.

Analyzing the charges on dimers without adsorbates, we can observe several changes. In the copper dimer, charges on both metal atoms and bridge oxygen changed depending on adsorbates. On the copper atoms the charge decreased in all cases (from approximately 0.700 to 0.670), while the charge on the bridge oxygen atom increased in the case of co-adsorption (from -0.564 to -0.436), decreased in the process of nitric oxide adsorption (from -0.564 to -0.650), and remained almost unchanged in the case of ammonia adsorption. In the iron dimer, especially in the case of nitric oxide adsorption and co-adsorption, the charge on metal atoms increased (on the average from 0.79 to approximately 0.94), the charge for bridge oxygen compared to the dimer without adsorbates decreased from -0.682 and its value is similar for all the adsorption processes (approximately -0.740). In the last of the dimers – the manganese dimer – we can

notice that the nitric oxide adsorption and co-adsorption caused an increase in charge on manganese metals (from approximately 0.960 to 1.014 on the average), whereas the adsorption of ammonia resulted in a decrease. The charge on bridge oxygen increased and is similar in all cases (approximately -0.767). Based on the above analysis it can be concluded that the charge redistribution differs significantly depending on a type of metal in the dimer structure and is not comparable even in the area of the same adsorbate.

The next analysis conducted for the obtained structures was the analysis which included the lengths and bond orders (Fig. 6). As mentioned before, significant differences can be seen in the analysis of bond orders even for dimers themselves. First of all, a change in bond orders for metals in a dimer deserves attention. In the copper system one can notice weakening of this interaction between Cu-Cu from 0.23 to approximately 0.19 and even 0.13 in the case of co-adsorption. Also the strength of the bond between the copper atom and bridge oxygen is significantly weakened, and the bond length increases for all adsorption processes (an increase in the range of 0.06–0.92 Å). In contrast, both in the case of the iron and manganese dimer, such a tendency is not observed. In the iron dimer, adsorption of nitric oxide and co-adsorption significantly (almost sixfold) weaken the interaction of metals with each other (from 1.215 to 0.23 and 0.26), while ammonia adsorption virtually does not

affect the order of this bond. Also, the lengths of bond of the iron atom with a bridge oxygen behave completely differently than in the copper dimer as the bonds become shortened by approximately 0.06 Å. Only in the case of ammonia adsorption on a metallic dimer bonding of the bridge oxygen to the metal atom to which ammonia is attached is slightly longer (0.12 Å). In the manganese

dimer, however, it can be observed that adsorption processes increase the bond order between manganese atoms from 0.107 to 0.160 for the adsorption of nitric oxide, 0.870 for the adsorption of ammonia and 0.176 for co-adsorption, which suggests an increase in interaction between metal atoms. The lengths of bridge oxygen-metal bonds are shortened.

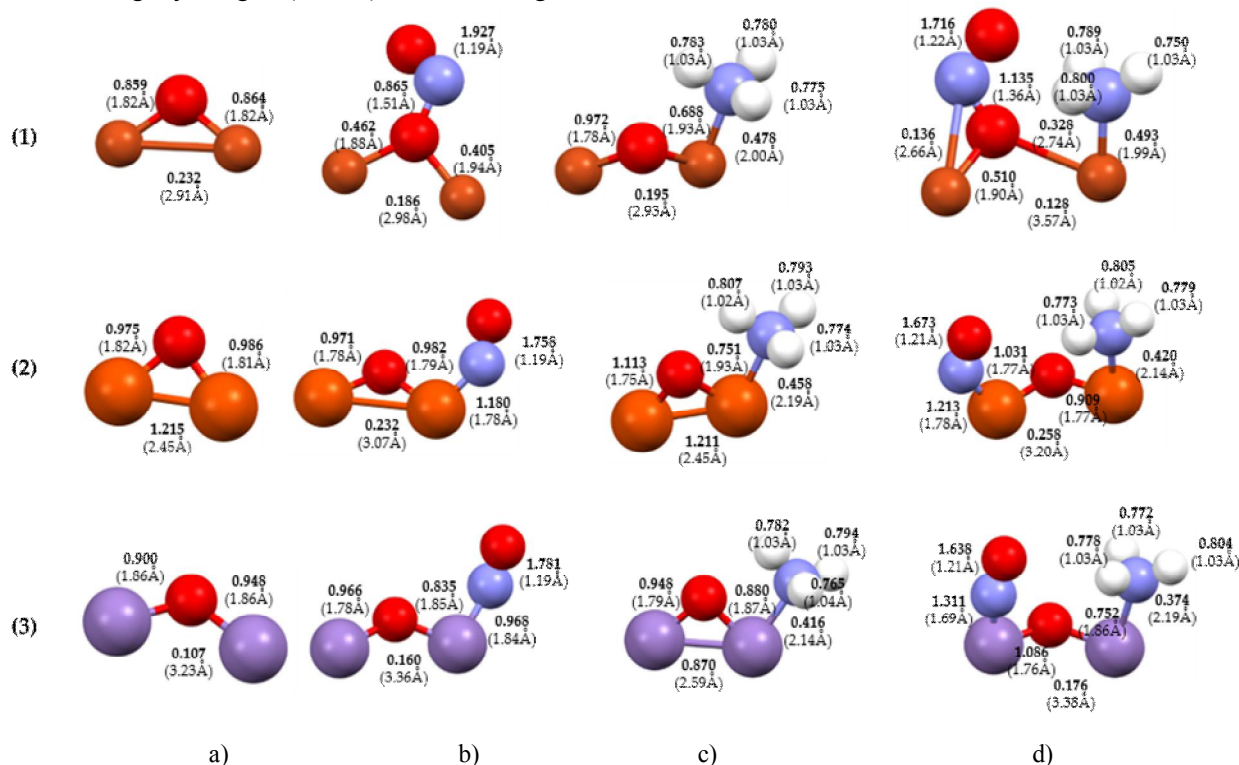


Fig. 6. Length and bond orders for metallic dimer: copper (1), iron (2) and manganese (3). Metal dimers (a), nitric oxide adsorption (b), ammonia adsorption (c), nitric oxide and ammonia adsorption (d)

Changes taking place in the bond orders and lengths of adsorbates compared to their free, unadsorbed molecules were also analyzed. For unadsorbed nitric oxide the bond order is 2.216 and the length is 1.18 Å, while for ammonia the bond order is 0.880 and the bond length is 1.03 Å, and they are the same for each of the hydrogen atoms. Comparing this with the adsorbed molecules, we can observe a repetitive pattern – the bond order of the adsorbed nitric oxide decreases on all dimers, and in the case of co-adsorption it is even lower than in the case of a single nitric oxide molecule adsorption. The bond length also undergoes changes and increases slightly, in the case of adsorption of only nitric oxide it increases by 0.01 Å and in the case of co-adsorption – by 0.03 Å for the iron and manganese dimer, by 0.04 Å – for the copper dimer. Such changes in the adsorbed molecule indicate the weakening of the nitrogen-oxygen bond, which in the further stage of the SCR reaction is essential for obtaining N₂ and H₂O. Regarding only the bond of

nitric oxide with the dimer, the weakest interaction (allowing further reactions with the adsorbates) demonstrates the nitrogen-bridge oxygen bond in the copper dimer (0.865), and the strongest – in the iron dimer (1.180), where nitrogen binds to the metal atom. In the case of coadsorption, the interaction of nitric oxide with the dimer is much stronger for all metals. In addition, the connection in the copper dimer takes place via a bridge oxygen atom and the metal atom. Comparing the orders and lengths of bonds in the unadsorbed and adsorbed ammonia molecule it can be noticed that in both single adsorption and co-adsorption the nitrogen-hydrogen bond order decreases while the bond length does not change. However, the strength of interaction of the nitrogen molecule is the weakest in the case of binding with the manganese dimer (approximately 0.360), and stronger for the copper and iron dimer (approximately 0.46).

Finally, vibration calculations were also performed for individual adsorbates (Figs. 7-9). The frequency values

presented in the drawings refer to harmonic and anharmonic vibrations, with necessary corrections. In all cases the vibration frequency is comparable between individual adsorbates and slightly different for different metals in the dimer. Nitric oxide vibrations (Figs. 7-9, a) in all cases are symmetrical stretching vibrations and their frequency successively amounts to 1700 cm^{-1} (1696 cm^{-1}) for the copper dimer, 1779 cm^{-1} (1773 cm^{-1}) for the copper dimer, 1746 cm^{-1} (1740 cm^{-1}) for the manganese dimer.

The values for anharmonic vibrations are given in brackets. In the case of ammonia adsorption (Figs. 7-9, b_{1-3}) three types of vibrations can be distinguished: one of a symmetrical stretching type and two of a scissor type. They amount to: $1198, 1591, 1664\text{ cm}^{-1}$ ($1032, 1586, 1641\text{ cm}^{-1}$) for the copper dimer; $1271, 1643, 1652\text{ cm}^{-1}$ ($1248, 1639, 1642\text{ cm}^{-1}$) for the iron dimer; $1288, 1650, 1655\text{ cm}^{-1}$ ($1287, 1648, 1651\text{ cm}^{-1}$) for the manganese dimer, respectively.

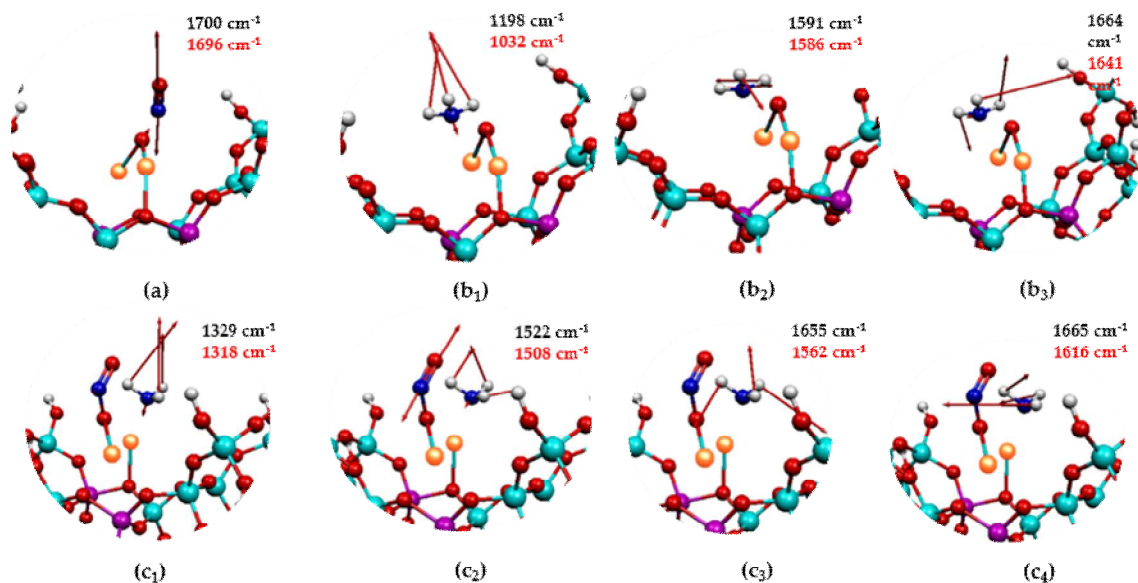


Fig. 7. Vibration for faujasite zeolite structures with copper dimer and adsorbates: nitric oxide (a), ammonia (b_{1-3}), nitric oxide and ammonia (c_{1-4}). Vibrations with harmonic (black) and anharmonic (red) approximation

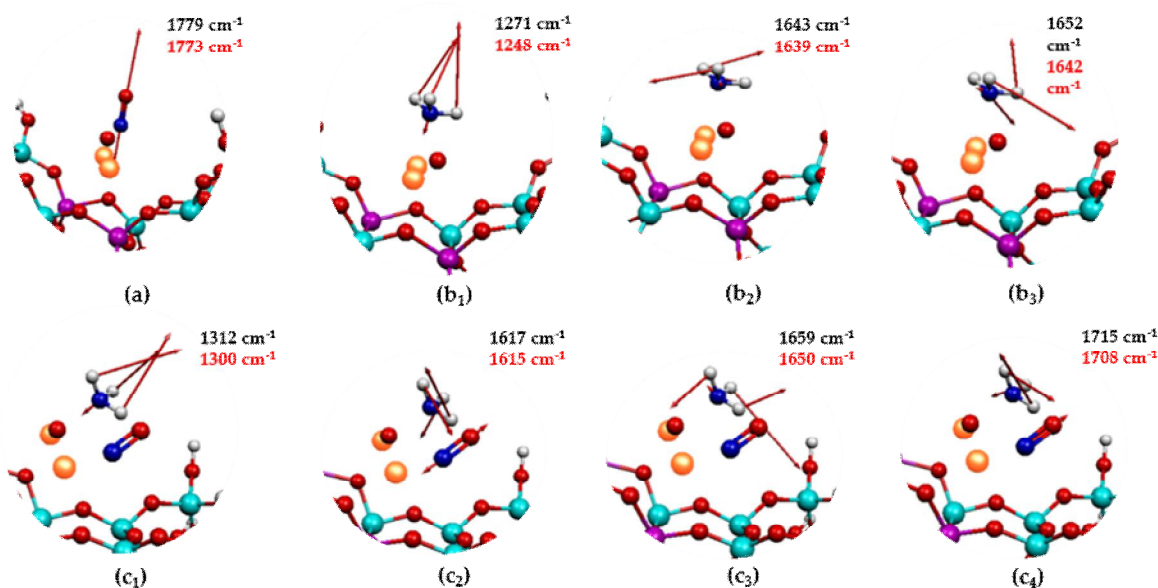


Fig. 8. Vibration for faujasite zeolite structures with iron dimer and adsorbates: nitric oxide (a), ammonia (b_{1-3}), nitric oxide and ammonia (c_{1-4}). Vibrations with harmonic (black) and anharmonic (red) approximation

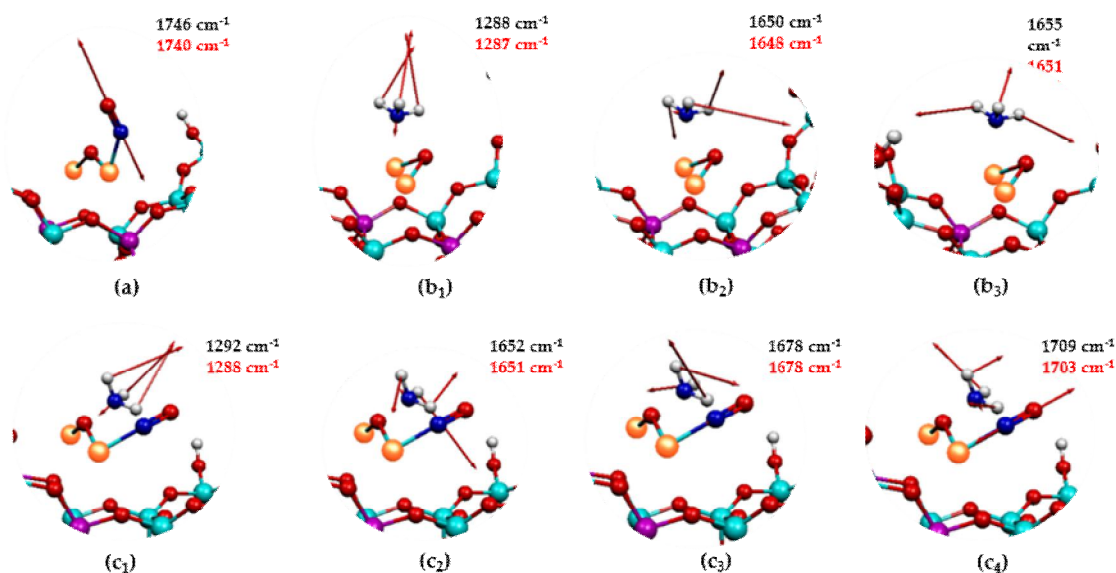


Fig. 9. Vibration for faujasite zeolite structures with manganese dimer and adsorbates: nitric oxide (a), ammonia (b₁₋₃), nitric oxide and ammonia (c₁₋₄). Vibrations with harmonic (black) and anharmonic (red) approximation

The last vibrations analyzed concern co-adsorption (Figs. 7-9, c₁₋₄). It can be observed that out of four characteristic vibrations, only one applies to the vibrations of both adsorbates (in the case of the iron dimer, the vibrations of both molecules exhibit two frequencies, but for one of them the vibration of nitric oxide is of low intensity compared to the vibrations of ammonia). The first vibration only for ammonia with the values of 1329 cm⁻¹ (1318 cm⁻¹, copper dimer), 1312 cm⁻¹ (1300 cm⁻¹, iron dimer), 1292 cm⁻¹ (1288 cm⁻¹, manganese dimer) is of a symmetrical stretching type, while the second vibration, depending on a type of the dimer, is of a different character. For the copper dimer 1655 cm⁻¹ (1562 cm⁻¹) these vibrations are of a scissor type, for the iron dimer 1659 cm⁻¹ (1650 cm⁻¹) these vibrations are oscillating vibrations and for the manganese dimer 1678 cm⁻¹ (1678 cm⁻¹) these vibrations are of a twisting type. When it comes to vibrations of both adsorbates at the same time, we can compare vibrations occurring in the copper and iron dimer, and vibrations in the iron and manganese dimer. Comparing vibrations between the copper and manganese dimer is difficult due to the lack of similar values. Comparing vibrations for the first two dimers, we are dealing with vibrations of two adsorbates with a frequency of 1522 cm⁻¹ (1508 cm⁻¹, copper dimer) and 1617 cm⁻¹ (1615 cm⁻¹, iron dimer). In both cases the nitric oxide exhibits symmetrical stretching vibrations, whereas ammonia – wagging vibrations for the copper dimer and twisting vibrations for the iron dimer. In the latter case, comparing the vibrations of both adsorbates in the iron dimer: 1715 cm⁻¹ (1708 cm⁻¹) and in the manganese dimer: 1709 cm⁻¹ (1703 cm⁻¹), the vibrations

for nitric oxide are also of a symmetrical stretching type, and ammonia in both cases makes scissor movements.

The difference in vibration values for nitric oxide can be significantly influenced by another mechanism of binding to the dimer (*via* bridge oxygen). Conducting further research and comparing it with experimental results would allow to confirm this type of mechanism on a real catalyst.

4. Conclusions

Dimers selected in the research (Cu, Fe and Mn) exhibit stability in the proposed zeolite fragment and the binding mechanism is the same regardless of the type of a metal atom. In the case of practically all types of adsorption (nitric oxide, ammonia and coadsorption of nitric oxide and ammonia) the process will occur spontaneously with the release of energy from the system. Due to the differences in atomic charges, the mechanism of binding of nitric oxide to the copper dimer occurs with the participation of the dimer bridge oxygen, whereas for the iron and manganese dimer – with the participation of one of the metal atoms in the dimer. The weakest interaction of adsorbates with a dimer was observed in the case of coadsorption of nitric oxide and ammonia on manganese, which may suggest that further conducting of the SCR process will be favoured on this catalyst.

These studies, together with the vibration analysis, provide a good basis for comparison with experimental results in order to confirm the presented adsorption mechanisms.

Acknowledgments

This theoretical work was supported by the PL-Grid Infrastructure.

References

- [1] Shelef M.: Chem. Rev. 1995, **95**, 209. <https://doi.org/10.1021/cr00033a008>
- [2] Yashnik S., Ismagilov Z.: Appl. Catal. B-Environ., 2015, **170**, 241. <https://doi.org/10.1016/j.apcatb.2015.01.021>
- [3] Rudolph J., Jacob C.R.: ACS Omega, 2019, **4**, 7987. <https://doi.org/10.1021/acsomega.9b00600>
- [4] Long R., Yang R.: J. Catal., 1999, **188**, 332. <https://doi.org/10.1006/jcat.1999.2674>
- [5] Schwidder M., Kumar M., Klementiev K. *et al.*: J. Catal., 2005, **231**, 314. <https://doi.org/10.1016/j.jcat.2005.01.031>
- [6] Grossale A., Nova L., Tronconi E.: Catal. Today, 2008, **136**, 18. <https://doi.org/10.1016/j.cattod.2007.10.117>
- [7] Schmieg S., Oh S., Kim C. *et al.*: Catal. Today, 2012, **184**, 252. <https://doi.org/10.1016/j.cattod.2011.10.034>
- [8] Blakeman P., Burkholder E., Chen H.-Y., *et al.*: Catal. Today, 2014, **231**, 56. <https://doi.org/10.1016/j.cattod.2013.10.047>
- [9] Sun Q., Gao Z., Chen H., Sachtler W.: J. Catal., 2011, **201**, 89. <https://doi.org/10.1006/jcat.2001.3228>
- [10] Heindrich F., Schmidt C., Loeffler E. *et al.*: J. Catal., 2002, **212**, 157. <https://doi.org/10.1006/jcat.2002.3775>
- [11] Kröcher O., Devadas M., Elsener M., *et al.*: Appl. Catal. B, 2006, **66**, 208. <https://doi.org/10.1016/j.apcatb.2006.03.012>
- [12] Ma A., Grünert W.: Chem. Commun., 1999, **1**, 71. <https://doi.org/10.1039/A807490I>
- [13] Santhosh K., Schwidder M., Grünert W., *et al.*: J. Catal., 2006, **239**, 173. <https://doi.org/10.1016/j.jcat.2006.01.024>
- [14] Rivallan M., Ricchiardi G., Bordiga S., Zecchina A.: J. Catal., 2009, **264**, 104. <https://doi.org/10.1016/j.jcat.2009.03.012>
- [15] Pirutko L., Chernyavsky V., Starokon E. *et al.*: Appl. Catal. B, 2009, **91**, 174. <https://doi.org/10.1016/j.apcatb.2009.05.021>
- [16] Fellah M., van Santen R., Onal I.: J. Phys. Chem. C, 2009, **113**, 15307. <https://doi.org/10.1021/jp904224h>
- [17] Yuranov I., Bulushev D., Renken A., Kiwi-Minsker L.: Appl. Catal. A, 2007, **319**, 128. <https://doi.org/10.1016/j.apcata.2006.11.023>
- [18] Czekaj I., Brandenberger S., Kröcher O.: Micropor. Mesopor. Mat., 2013, **169**, 97. <https://doi.org/10.1016/j.micromeso.2012.10.018>
- [19] Ehrlich H., Schwieger W., Jahnisch K.: Appl. Catal. A-Gen., 2004, **272**, 311. <https://doi.org/10.1016/j.apcata.2004.06.003>
- [20] Battiston A., Bitter J., Koningsberger D.: J. Catal., 2003, **218**, 163. [https://doi.org/10.1016/S0021-9517\(03\)00120-9](https://doi.org/10.1016/S0021-9517(03)00120-9)
- [21] Chen H., Sachtler W.: Catal. Today, 1998, **42**, 73. [https://doi.org/10.1016/S0920-5861\(98\)00078-9](https://doi.org/10.1016/S0920-5861(98)00078-9)
- [22] Joyner R., Stockenhuber M.: J. Phys. Chem. B, 1999, **103**, 5963. <https://doi.org/10.1021/jp990978m>
- [23] Joyner R., Stockenhuber M.: Catal. Lett., 1997, **45**, 15. <https://doi.org/10.1023/A:1019063511784>
- [24] Krishna K., Makkee M.: Catal. Today, 2006, **114**, 23. <https://doi.org/10.1016/j.cattod.2006.02.002>
- [25] Hensen E., Zhu Q., van Santen R.: J. Catal., 2003, **220**, 260. <https://doi.org/10.1016/j.jcat.2003.09.001>
- [26] Zecchina A., Rivallan M., Berlier G., *et al.*: Phys. Chem. Chem. Phys., 2007, **9**, 3483. <https://doi.org/10.1039/B703445H>
- [27] Sun K., Xia H., Feng Z., *et al.*: J. Catal., 2008, **254**, 383. <https://doi.org/10.1016/j.jcat.2008.01.017>
- [28] Panov G., Uriarte A., Rodkin M., Sobolev V.: Catal. Today, 1998, **41**, 365. [https://doi.org/10.1016/S0920-5861\(98\)00026-1](https://doi.org/10.1016/S0920-5861(98)00026-1)
- [29] El-Malki E., van Santen R., Sachtler W.: J. Catal., 2000, **196**, 212. <https://doi.org/10.1006/jcat.2000.3034>
- [30] Perez-Ramirez J.: J. Catal., 2004, **227**, 512. <https://doi.org/10.1016/j.jcat.2004.08.005>
- [31] Pirngruber G., Roy P.: Catal. Today, 2005, **110**, 199. <https://doi.org/10.1016/j.cattod.2005.09.023>
- [32] Moreno-González M., Hueso B., Boronat M., *et al.*: J. Phys. Chem. Lett., 2015, **6**, 1011. <https://doi.org/10.1021/acs.jpcclett.5b00069>
- [33] Zhang R., McEwen J.-S., Kollár M. *et al.*: ACS Catal., 2014, **4**, 4093. <https://doi.org/10.1021/cs500563s>
- [34] Zhang R., Li H., McEwen J.-S.: J. Phys. Chem. C, 2017, **121**, 25759. <https://doi.org/10.1021/acs.jpcc.7b04309>
- [35] Paolucci C., Parekh A., Khurana I. *et al.*: J. Am. Chem. Soc., 2016, **138**, 6028. <https://doi.org/10.1021/jacs.6b02651>
- [36] Kerkeni B., Berthout D., Berthomieu D. *et al.*: J. Phys. Chem. C, 2018, **122**, 16741. <https://doi.org/10.1021/acs.jpcc.8b03572>
- [37] Chen P., Khetan A., Jabłońska M. *et al.*: Appl. Catal. B-Environ., 2018, **237**, 263. <https://doi.org/10.1016/j.apcatb.2018.05.091>
- [38] Zhang R., Anderst E., Groden K., McEwen J.-S.: Ind. Eng. Chem. Res., 2018, **57**, 13396. <https://doi.org/10.1021/acs.iecr.8b03643>
- [39] Baran R., Valentin L., Krafft J.-M. *et al.*: Phys. Chem. Chem. Phys., 2017, **19**, 13553. <https://doi.org/10.1039/C7CP02096A>
- [40] Ettireddy P., Ettireddy N., Mamedov S. *et al.*: Appl. Catal. B, 2007, **76**, 123. <https://doi.org/10.1016/j.apcatb.2007.05.010>
- [41] Liu F., He H., Ding Y., Zhang C.: Appl. Catal. B, 2009, **93**, 194. <https://doi.org/10.1016/j.apcatb.2009.09.029>
- [42] Liang X., Li J., Lin Q., Sun K.: Catal. Commun., 2007, **8**, 1901. <https://doi.org/10.1016/j.catcom.2007.03.006>
- [43] Samojedan B., Motak M., Grzybek T.: C. R. Chim., 2015, **18**, 1049. <https://doi.org/10.1016/j.crci.2015.04.001>
- [44] Favez J.-Y., Weilenmann M., Stilli J.: Atmos. Environ., 2009, **43**, 996. <https://doi.org/10.1016/j.atmosenv.2008.03.037>
- [45] Borfecchia E., Lomachenko K., Giordanino F. *et al.*: Chem. Sci., 2015, **6**, 548. <https://doi.org/10.1039/C4SC02907K>
- [46] Dzwigaj S., Massiani P., Davidson A., Che M.: J. Mol. Catal. A-Chem., 2000, **155**, 169. [https://doi.org/10.1016/S1381-1169\(99\)00332-5](https://doi.org/10.1016/S1381-1169(99)00332-5)
- [47] Dzwigaj S., Matsuoka M., Franck R. *et al.*: J. Phys. Chem. B, 1998, **102**, 6309. <https://doi.org/10.1021/jp981454+>
- [48] Xu W., Zhang G., Chen H. *et al.*: Chinese J. Catal., 2018, **39**, 118. [https://doi.org/10.1016/S1872-2067\(17\)62983-8](https://doi.org/10.1016/S1872-2067(17)62983-8)
- [49] Gao F., Kwak J., Szanyi J., Peden C.: Top. Catal., 2013, **56**, 1441. <https://doi.org/10.1007/s11244-013-0145-8>
- [50] Janssens T., Falsig H., Lundegaard L. *et al.*: ACS Catal., 2015, **5**, 2832. <https://doi.org/10.1021/cs501673g>
- [51] Paolucci C., Verma A., Bates S. *et al.*: Angew. Chem. Int. Edit., 2014, **53**, 11828. <https://doi.org/10.1002/anie.201407030>
- [52] Mao Y., Wang Z., Wang H.-F., Hu P.: ACS Catal., 2016, **6**, 7882. <https://doi.org/10.1021/acscatal.6b01449>
- [53] Günter T., Carvalho H., Doronkin D. *et al.*: Chem. Commun., 2015, **51**, 9227. <https://doi.org/10.1039/C5CC01758K>
- [54] Mao Y., Wang H.-F., Hu P.: Int. J. Quantum Chem., 2015, **115**, 618. <https://doi.org/10.1002/qua.24844>
- [55] Brüggemann T., Keil F.: J. Phys. Chem. C, 2011, **115**, 23854. <https://doi.org/10.1021/jp206931z>
- [56] Hermann K., Pettersson L., Casida M. *et al.*: StoBe-deMon; deMon Software: Stockholm, Berlin 2005. <http://www.fhi-berlin.mpg.de/KHsoftware/StoBe/>
- [57] Perdew J., Burke K., Ernzerhof M.: Phys. Rev. Lett., 1996, **77**, 3865. <https://doi.org/10.1103/PhysRevLett.77.3865>
- [58] Hammer B., Hansen L., Nørskov J.: Phys. Rev. B, 1999, **59**, 7413. <https://doi.org/10.1103/PhysRevB.59.7413>

- [59] Broclawik E., Salahub D.: J. Mol. Catal., 1993, **82**, 117.
[https://doi.org/10.1016/0304-5102\(93\)80028-S](https://doi.org/10.1016/0304-5102(93)80028-S)
- [60] Jasiński R.: React. Kinet. Mech. Catal., 2016, **119**, 49.
<https://doi.org/10.1007/s11144-016-1038-1>
- [61] Mulliken R.: J. Chem. Phys., 1955, **23**, 1833.
<https://doi.org/10.1063/1.1740589>
- [62] Mayer I.: Chem. Phys. Lett., 1983, **97**, 270.
[https://doi.org/10.1016/0009-2614\(83\)80005-0](https://doi.org/10.1016/0009-2614(83)80005-0)
- [63] Mayer I.: J. Mol. Struct.-THEOCHEM, 1987, **149**, 81.
[https://doi.org/10.1016/0166-1280\(87\)80048-9](https://doi.org/10.1016/0166-1280(87)80048-9)
- [64] Friedrich C.: Geometrische, elektronische und vibronische Eigenschaften der reinen und defektbehafteten V₂O₅(010)-Oberfläche und deren Wechselwirkung mit Adsorbaten, FU, Berlin 2004.
<https://doi.org/10.17169/refubium-18117>
- [65] <http://www.iza-structure.org/databases/>. (accessed on 03.02.2020)

Received: February 02, 2020 / Revised: March 20, 2020 /
Accepted: September 01, 2020

ТЕОРЕТИЧНІ ДОСЛІДЖЕННЯ DeNO_x SCR НА КАТАЛІЗАТОРАХ Cu-, Fe- ТА Mn-FAU

Анотація. Проведено неемпіричні розрахунки на основі теорії функціональної щільності. Використана кластерна модель фожаситної цеолітової структури (Al₂Si₂₂O₆₆H₃₆) з частинками металу, адсорбованими на алюмінієвих центрах. Процеси індивідуальної та ко-адсорбції NO і NH₃ вивчені на наночастинках металів, пов'язаних у цеолітові кластери. Для визначення можливих шляхів реакції deNO_x проаналізовано конфігурації, електронну структуру (заряди, порядки зв'язку) та частоти вібрацій. У відповідності до попередніх досліджень комплексів заліза розглянуті димери M₂O (M = Cu, Mn або Fe).

Ключові слова: цеоліти, FAU, deNO_x, вібраційна структура, SCR, кластерна модель.